Myelin-reactive B cells exacerbate the severity of CD4$^+$ T cell-driven CNS autoimmunity in an IL-23-dependent manner.

Mohamed Reda Fazazi[1], Prenitha Mercy Ignatius Arokia Doss[1], Resel Pereira[2], Neva Fudge[3,4], Aryan Regmi[2,5], Irshad Akbar[1], Asmita Pradeep Yeola[1], Benoit Mailhot[1], Joanie Baillargeon[1], Philippe Grenier[6], Nicolas Bertrand[6,7], Steve Lacroix[1,8], Craig S. Moore[3,4], Olga L. Rojas[2,5], Manu Rangachari[1,8,9].

[1] axe Neurosciences, Centre de recherche du CHU de Québec – Université Laval, Pavillon CHUL, 2705 boul Laurier, Quebec City, QC, CANADA G1V 4G2; [2] Krembil Research Institute, University Health Network, Toronto ON CANADA M5T 0S8; [3] Division of BioMedical Sciences and [4] Department of Neurology, Faculty of Medicine, Memorial University of Newfoundland, St. John's NL, CANADA, A1B 3V6; [5] Department of Immunology, University of Toronto, Toronto ON, CANADA, M5S 1A1; [6] axe Endocrinologie et nephrologie, Centre de recherche du CHU de Québec – Université Laval, Pavillon CHUL, 2705 boul Laurier, Quebec City, QC, CANADA G1V 4G2; [7] Faculty of Pharmacy, Laval University, 1050 ave de la Médecine, Quebec City, CANADA; [8] Department of Molecular Medicine, Faculty of Medicine, Laval University, 1050 ave de la Médecine, Quebec City, CANADA; [9] Corresponding author.

Abstract

Multiple sclerosis (MS) is an autoimmune disorder of the central nervous system (CNS) that has traditionally been considered a T cell-mediated disease. However, accumulating evidence points to a crucial role for B cells in disease processes. IgH$^{[MOG]}$ mice possess a transgenic immunoglobulin heavy chain derived from a monoclonal antibody specific to myelin oligodendrocyte glycoprotein (MOG), a key target for autoimmune responses. Here, using the experimental autoimmune encephalomyelitis (EAE) model of MS, we investigated the susceptibility of IgH$^{[MOG]}$ mice to CD4^{+} T cell-driven disease that was induced by active immunization with MOG$_{[35-55]}$ autoantigen. We found that immunized IgH$^{[MOG]}$ mice rapidly developed severe EAE. While the frequency and absolute number of CNS-infiltrating B cells was similar between WT and IgH$^{[MOG]}$ mice, a greater frequency of class-switched and inflammatory cytokine-positive B cells were seen in the IgH$^{[MOG]}$ CNS. We observed an increased presence of class-switched and inflammatory cytokine-positive B cells in the IgH$^{[MOG]}$ CNS, as well as a greater frequency of IL-17- and GM-CSF-producing CD4^{+} T cells. Production of the Th17 maintenance factor IL-23 was increased from IgH$^{[MOG]}$ CNS-infiltrating B cells, and *in vivo* blockade of IL-23p19 strongly attenuated disease severity in IgH$^{[MOG]}$ mice. Strikingly, we observed an increased frequency of PD-1^{+}CXCR5^{-} T peripheral helper (Tph)-like cells in the CNS of IgH$^{[MOG]}$ mice and we also found that the meninges of immunized IgH$^{[MOG]}$ mice were characterized by an accumulation of tertiary lymphoid organs. Both Tph accumulation in the CNS, as well as meningeal inflammation, were again sharply

reduced upon IL-23p19 blockade *in vivo*. Intriguingly, the expression of *IL23a* transcript in the cerebrospinal fluid of MS-affected individuals was positively correlated with the frequency of B cells. Altogether, these data show that MOG-specific B cells contribute to severe $CD4^+$ T cell-driven EAE by promoting CNS accumulation of Th17 and Tph cells, as well as tertiary lymphoid organs in the CNS meninges, in an IL-23 dependent manner.

Keywords: experimental autoimmune encephalomyelitis, multiple sclerosis, B cell, $CD4^+$ T cell, myelin oligodendrocyte glycoprotein (MOG), IgH[MOG], 1C6, non-obese diabetic (NOD), Th17, IL-23, T-peripheral helper cells (Tph cells), tertiary lymphoid organ.

Introduction

Multiple sclerosis (MS) is a chronic autoimmune disease in which the adaptive immune system launches an attack against central nervous system (CNS) proteins, such as myelin. MS affects more than 2 million people worldwide [1]. Approximately 80% of patients present an initially relapsing-remitting (RR) disease course for which there are now more than 10 disease-modifying therapies available. However, 30-60% of these RR patients will eventually transition to a chronically worsening secondary progressive (SP) phase, for which treatment options are limited [2]. Pathophysiological mechanisms in progressive MS are thus of intense current interest [3].

T cells, and $CD4^+$ T cells in particular, have historically been the most intensively studied players in the immune pathogenesis of MS. However, it has become increasingly clear that B cells additionally play important roles in MS pathogenesis. Clonally expanded B cells are present in the cerebrospinal fluid (CSF) and MS plaques[4-6], and the presence of meningeal follicles adjacent to cortical lesions is associated with disease progression[7,8]. Further, antibodies against myelin oligodendrocyte glycoprotein (MOG), a key component of myelin, were found in active MS lesions [9]. Crucially, the B cell-targeting anti-CD20 drugs rituximab[10], ocrelizumab[11] and ofatumumab[12] improve RRMS, and ocrelizumab is the only FDA approved drug for primary progressive MS[13]. Curiously, though, antibody-secreting plasmablasts do not express CD20 (ref [14]). This suggests that the pathogenic role of B cells in MS might lie less with the generation of

autoantibodies, and more with their capacity to interact with other immune cell types, such as T cells.

Experimental autoimmune encephalomyelitis (EAE) is an animal disease that recapitulates many of the immune aspects of MS pathogenesis. Use of this model has helped us to understand the role of T cells, and $CD4^+$ T cells in particular, in the initiation and maintenance of autoreactive inflammation in the CNS [15]. However, studies using the transgenic $IgH^{[MOG]}$ mouse strain have indicated that B cells may also play a crucial role in EAE pathology[16-18]. These mice (also known as "Th") express a knocked-in IgH chain derived from a MOG-specific antibody; thus, around 30% of their B cells are therefore specific for MOG protein[16]. $IgH^{[MOG]}$ animals develop severe EAE when immunized with either whole MOG protein[16] or with its extracellular domain ($MOG_{[1-125]}$)[19], indicating an important role for MOG-reactive B cells in neuroimmune processes. Further, they develop spontaneous EAE when crossed to myelin peptide-specific T cell receptor transgenic lines on the B6 (ref [17]) and SJL/J[18] backgrounds. Indeed, while "T cell help" is required for the full activation of B cells in the majority of cases, there is increasing evidence that B cells can reciprocally promote effector T cell responses, notably those of the Th17 lineage[20-24]. However, the potential mechanisms by which MOG-reactive B cells facilitate T cell-driven pathogenicity, such as in class II-restricted peptide immunization models of EAE, remain incompletely understood.

Here, we studied the co-operative role of B cells and T cells in CNS autoimmunity using $IgH^{[MOG]}$ mice on the non-obese diabetic (NOD) genetic

background. We immunized these, and wildtype (WT) NOD mice, with $MOG_{[35-55]}$, a MHC class II-restricted peptide that obligatorily drives a $CD4^+$ T cell response. While WT NOD mice gradually develop a relapsing chronic form of EAE over the course of 80-100 days when immunized with $MOG_{[35-55]}$ [25], we observed that $IgH^{[MOG]}$ mice developed a rapid, severe form of EAE that was characterized by demyelination and inflammation of the CNS. Severe disease in these mice was accompanied by an increase in the frequency of CNS-infiltrating T cells that produced IL-17 and GM-CSF, but not IFNγ; further, the $IgH^{[MOG]}$ CNS meninges was characterized by the presence of colocalized clusters of $CD4^+$ T cells, B cells and $CD11c^+$ dendritic cells (DCs), as well as expansion of the underlying extracellular matrix (ECM) that resembled tertiary lymphoid organs (TLOs). Production of the Th17 maintenance factor IL-23 was increased from CNS-infiltrating B cells in $IgH^{[MOG]}$ mice; *in vivo* blockade of IL-23p19 rescued the severe EAE phenotype in these mice, and also reduced the presence of meningeal TLOs and the frequency of $PD1^+CXCR5^-$ "T peripheral helper-like cells", a recently described effector T cell subset that associates with B cells in the inflamed synovium in rheumatoid arthritis (RA) [26]. Intriguingly, Il23p19 (*Il23a*) transcript expression in the cerebrospinal fluid of MS-affected individuals was correlated to the frequency of B cells. Together, our results demonstrate that MOG-specific B cells play a crucial role in augmenting $CD4^+$ T cell-driven EAE in an IL-23-dependent manner.

Results

IgH$^{[MOG]}$ mice develop severe EAE upon active immunization with MOG$_{[35-55]}$

When immunized with MOG$_{[35-55]}$, wildtype WT NOD mice display a disease course characterized by relapse remitting disease in the early phase that transitions to a chronic worsening phase in some animals [25]. NOD-EAE has thus been considered a possible model of SPMS [27,28], though others argue against this interpretation [29]. We confirmed that MOG$_{[35-55]}$-immunized WT NOD mice develop disease characterized by relatively mild symptoms over the first ~100 days (Supplemental Figure 1A). We next compared the development of EAE between NOD-background WT and IgH$^{[MOG]}$ mice upon MOG$_{[35-55]}$ immunization. Both male and female IgH$^{[MOG]}$ mice developed extremely severe disease within 25 days (Figure 1A), with a substantial frequency of these mice attaining ethical endpoints (10/14 IgH[MOG] males vs. 0/14 WT males, p=0.0002; 12/16 IgH$^{[MOG]}$ females vs. 0/16 WT females, p<0.0001). Histopathological analyses revealed increased lymphocyte infiltration and demyelination in the spinal cords of IgH$^{[MOG]}$ mice relative to controls (Figure 1B).

We next examined peripheral T cell responses prior to disease onset. No differences in IL-17 or IFNγ were detected by either *ex vivo* flow cytometry (Figure 1C) or by ELISA after MOG$_{[35-55]}$ peptide recall (Supplemental Figure 1B). While the cervical LNs are a potential site of T cell reactivation in MS [30], we observed limited production of IL-17 and IFNγ in this compartment; while a large proportion of CD4^{+} T cells in cervical LNs were positive for TNFα, no differences

were detected between WT and IgH$^{[MOG]}$ (Supplemental Figure 1C). To identify a possible role for IgH$^{[MOG]}$ B cells in directly driving T cell responses, we pulsed IgH[MOG] or WT B cells with MOG$_{[35-55]}$ and co-cocultured them with MOG$_{[35-55]}$-specific 1C6 transgenic T cells[31-33]. No differences were observed in T cell proliferation (Supplemental Figure 1D), indicating that IgH$^{[MOG]}$ B cells were not intrinsically better at presenting antigen to T cells.

Antigen-specific antibody (Ab) secretion is the primary function of B cells. Further, oligoclonal immunoglobulin (Ig) banding in cerebrospinal fluid (CSF) is an important diagnostic marker for MS [34]. However, no differences in MOG-specific circulating IgG were found in IgH$^{[MOG]}$ serum relative to controls (Figure 1D), suggesting that severe disease in transgenic animals was not accompanied by an increase in MOG-specific autoantibodies. Together, these data showed that the presence of myelin-reactive B cells can exacerbate CNS autoimmunity and tissue damage when EAE is induced in a CD4^{+} T cell dependent manner. However, increased disease severity was unrelated to increased MOG antibody production or to an increased capacity of IgH$^{[MOG]}$ B cells to facilitate antigen presentation to MOG$_{[35-55]}$-specific CD4^{+} T cells.

Increased presence of immune cells in the CNS of immunized IgH$^{[MOG]}$ mice.

Target organ-infiltrating immune cells are essential to the pathogenesis of autoimmune disease. We therefore enumerated the frequency and absolute number of CNS-infiltrating immune cells – CD19^{+} B cells, CD4^{+} T cells, CD8^{+} T

cells, $CD11c^+$ dendritic cells (DCs), $CD11b^+CD11c^-$ macrophages and $Ly6G^+$ neutrophils – in immunized WT and $IgH^{[MOG]}$ mice. The relative frequencies and absolute numbers of $CD4^+$ T cells, $CD8^+$ T cells, DCs, macrophages and neutrophils were significantly increased in the CNS of $IgH^{[MOG]}$ mice relative to WT (Figure 2A).

Interestingly, despite having an antigenic repertoire heavily skewed towards MOG reactivity, immunized $IgH^{[MOG]}$ mice did not display an increase in frequency or absolute number (Figure 2A) of B cells in the CNS. We therefore assessed whether there might be differences in the proportion of functional B cell subsets between the groups. Indeed, we observed a stark increase in the frequency of class-switched (CS) IgM^-IgD^- B cells in the CNS (Figure 2B) of $IgH^{[MOG]}$ mice, which was accompanied by a decrease in the frequency of immature and mature B cells. In line with our finding that serum MOG-specific IgG was comparable between WT and $IgH^{[MOG]}$, we observed no differences in B cell subpopulation frequency in the spleen (Supplemental Fig 2A). Further, we observed no difference in MHC class II expression between CNS-infiltrating WT and $IgH^{[MOG]}$ B cells (Supplemental Fig 2B). On the other hand, an increase in $GL\text{-}7^+Fas^+$ germinal center (GC) B cells was seen in the $IgH^{[MOG]}$ CNS (Supplemental Figure 2C).

B cells can generate canonical inflammatory cytokines such as IL-6 (ref [35]), TNFα [36] and GM-CSF [37], with their production of such cytokines being linked to worsened outcomes in MS. We observed that a significantly greater proportion of $IgH^{[MOG]}$ CNS B cells produced these cytokines as compared to WT

counterparts, with the differences in IL-6 and TNFα being most apparent (Fig 2C). Altogether, these data point to qualitative differences between B cells in from the CNS of immunized WT versus IgH$^{[MOG]}$ mice, as well as a quantitative increase of T cells and innate immune cells.

Increased frequency of IL-17 and GM-CSF-positive CD4^{+} T cells in IgH$^{[MOG]}$ CNS.

As we had observed an elevated frequency of CD4^{+} T cells in the CNS of sick IgH$^{[MOG]}$ mice, we next examined the capacity of these cells to produce inflammatory Th1 and Th17 cytokines by flow cytometry, due to the well-established role of these CD4^{+} effector T cell subsets in EAE [38]. We observed no differences between IgH$^{[MOG]}$ and WT CD4^{+} T cells in their production of the IFNγ and TNFα in the CNS (Figure 3A). By contrast we saw a strong upregulation of IL-17 production from CNS-infiltrating CD4^{+} T cells from IgH$^{[MOG]}$ at disease endpoint. Notably, production of GM-CSF, a key pathogenic cytokine implicated in Th17-driven tissue inflammation, was also augmented in IgH$^{[MOG]}$ CD4^{+} T cells. These findings indicated that Th17 responses were specifically promoted in the CNS of immunized IgH$^{[MOG]}$ mice.

Accumulation of meningeal TLOs in IgH$^{[MOG]}$ mice

Meningeal TLOs have been documented in progressive MS and their presence correlates with poor outcomes [7,39]. Their presence in EAE is dependent on

murine genetic background and the manner of disease induction; while TLOs arise upon active immunization of SJL/J mice with $PLP_{[139-151]}$ [40], they do not appear in $MOG_{[35-55]}$-immunized C57BL/6J mice, rather arising only upon adoptive transfer of Th17 cells [41]. Whether or not they are a feature of NOD-EAE is as-yet unknown. As B cells are crucial to TLO formation[41], we assessed their presence in WT versus $IgH^{[MOG]}$ mice. Strikingly, we observed clustering of $CD4^+$ T cells, B cells and $CD11c^+$ DCs of varying magnitude in the brain and spinal cord of $IgH^{[MOG]}$ relative to WT mice. In the brain, meningeal clustering was chiefly observed in cerebellar fissures (Figure 3B).

TLOs are defined as tissue immune cell aggregates organized within a stroma cell network in inflamed non-lymphoid tissues. We found an increase of elaborate stroma network near the meninges in $IgH^{[MOG]}$ mice as demonstrated by the organized expansion of fibronectin, PDGFRαβa/b IF staining underneath the B cell clustering (Figure 3C). Together, these data demonstrate that TLOs accumulate in the meninges of $MOG_{[35-55]}$-immunized $IgH^{[MOG]}$ mice.

Augmented IL-23 production by $IgH^{[MOG]}$ mice leads to exacerbated disease

Our findings led us to investigate whether $IgH^{[MOG]}$ B cells may be characterized by increased production of the Th17 stabilization factor IL-23, which is essential to Th17 pathogenicity *in vivo* [42,43] and which can be secreted by human B cells[44]. The frequency of B cells co-expressing both chains of IL-23 ($p40^+p19^+$) was strongly upregulated in the $IgH^{[MOG]}$ CNS, despite showing no differences in co-

expression of the chains of the related cytokine, and Th1 differentiation factor, IL-12 ($p40^+p35^+$) (Figure 4A). Use of an antibody that detected IL-23 heterodimer confirmed that CNS $IgH^{[MOG]}$ B cells show higher expression of this cytokine (Figure 4B). As DCs are considered a major source of IL-23 (ref [45]), we investigated whether their capacity to generate this cytokine differed between WT and $IgH^{[MOG]}$ CNS; however, no differences were observed nor between WT and $IgH^{[MOG]}$ astrocytes[46] or microglia (Supplemental Figure 3A).

The robust upregulation of IL-23 by B cells in the $IgH^{[MOG]}$ CNS led us to ask whether it might be essential for the exacerbated disease seen in these animals. We therefore actively immunized $IgH^{[MOG]}$ mice and administered either anti-IL-23p19 blocking antibody[47] or isotype control. *In vivo* blockade abrogated severe EAE (Figure 4C), characterized by reduced lymphocyte infiltration and demyelination in the spinal cord (Figure 4D). Further, CNS-infiltrating $CD4^+$ T cells from anti-p19-treated $IgH^{[MOG]}$ mice showed decreased IL-17, and a trend towards reduced GM-CSF expression (Figure 4E); however, no differences in IFNγ production between T cells from anti-19 or isotype-treated mice were observed. In sum, these data show that excessive production of IL-23 by $IgH^{[MOG]}$ may underpin the severe pathology observed in these animals.

T peripheral helper (Tph)-like cells accumulate in the $IgH^{[MOG]}$ CNS

T follicular helper (Tfh) cells play a critical role in germinal center formation and B cell immune activation, and were recently shown to collaborate with B cells in

264 driving Th17-dependent EAE [48]. We therefore examined the presence of PD-
265 1^{+}CXCR5^{+} Tfh cells in splenic and CNS tissues from WT and IgH$^{[MOG]}$ mice. Tfh
266 were relatively rare in all cases (Figure 5A). Intriguingly, we instead observed a
267 increase in PD-1^{+}CXCR5^{-} CD4^{+} T cells in the IgH$^{[MOG]}$ CNS (Figure 5A). These
268 cells were reminiscent of the recently discovered "T peripheral helper" (Tph) cell
269 subset [26,49]. Originally discovered in the context of rheumatoid arthritis (RA), Tph
270 are recruited to the inflamed synovium, where they associate with B cells. They
271 are distinct from Tfh[26], and indeed we found that PD-1^{+}CXCR5^{-} cells from both
272 WT and IgH$^{[MOG]}$ mice were negative for the Tfh master transcription factor Bcl6
273 (ref [50]; Supplemental Figure 4A). While present in human RA [26,49] and lupus [51],
274 evidence for the accumulation of Tph in murine autoimmune disease is, thus far,
275 limited. Interestingly the frequency of PD-1^{+}CXCR5^{-} CD4^{+} T cells was higher at
276 the peak of EAE in IgH$^{[MOG]}$ mice as opposed to at onset or recovery (Figure 5B).
277 In addition to being PD-1^{+}CXCR5^{-}Bcl6^{-}, Tph are characterized as highly
278 positive for ICOS, CXCL13 and IL-21 (ref [26]). We therefore compared expression
279 of these markers between CNS-infiltrating PD-1^{neg} and PD-1^{+} CD4^{+} T cells of
280 both WT and IgH$^{[MOG]}$ mice. Expression of all three markers was upregulated in
281 the PD-1^{+} subpopulation in both WT and IgH$^{[MOG]}$ (Figure 5C), showing that CNS-
282 infiltrating PD1^{+}CXCR5^{-} cells express known Tph markers in the context of NOD-
283 EAE. By contrast, there was no difference in Bcl6 expression between PD-1^{+} and
284 PD-1^{-} cells (Supplemental Figure 4B) Interestingly, expression of IL-21 was
285 significantly higher in IgH$^{[MOG]}$ Tph-like cells relative to WT (Figure 5D).

Altogether, our data indicate that Tph-like cells accumulate in the CNS of EAE animals in the presence of MOG-specific B cells.

IL-23 is required for TLO formation and Tph recruitment

As Th17 cells are crucial to TLO formation[41], and as we had shown that the Th17 lineage maintenance factor IL-23 is obligatory for severe EAE in IgH$^{[MOG]}$ mice (Figure 4C), we next examined the effects of IL-23 blockade on the presence of TLOs in the meninges. Administration of anti-IL23p19 diminished the number of lymphocyte clusters in the meninges of IgH$^{[MOG]}$ mice (Figure 6A). Concomitantly, we observed a decrease in the intricate ECM network underneath, suggesting a decrease in meningeal TLOs in IgH$^{[MOG]}$ mice after administration of anti-IL23p19 (Figure 6B). We next examined whether *in vivo* depletion of IL-23 could impact Tph frequency. Indeed, the frequency of Tph was reduced in the CNS, but not spleen, of immunized IgH$^{[MOG]}$ treated with anti-p19 (Figure 6C). Therefore, we concluded that expression of IL-23 in IgH$^{[MOG]}$ underpinned not only severe disease, but also meningeal inflammation as well as recruitment of Tph to the CNS.

IL-23 expression in MS CSF correlates with the presence of B cells

The cerebrospinal fluid is a useful proxy for pathologic processes within the CNS parenchyma[52] and is routinely sampled in MS diagnosis. We therefore asked whether expression of IL-23p19 transcript in the CSF of MS-affected individuals were altered in relation to the presence of B cells. We examined the

CSF of 11 MS patients for expression of *Il23a* (IL-23p19 gene name) and correlated this to the frequency of $CD19^+$ B cells in the CSF of the same individuals. A robust correlation was identified (Spearman r = 0.7107) between *IL23a* and the proportion of $CD45^+$ leukocytes that were $CD19^+$ (Fig. 6D).

Discussion

The role of $CD4^+$ T cells in the autoimmune pathogenesis of MS is well-established: genome-wide association studies (GWAS) have revealed that polymorphisms in the human leukocyte antigen class II region are strongly associated with MS susceptibility [53], and many of the current treatments of MS are believed to target T cell responses [54-56]. However, the success of the B cell-depleting drug ocrelizumab in both RRMS and PPMS has intensified recent interest in the contribution of B cells to disease processes [57].

$IgH^{[MOG]}$ mice were initially described on the C57BL/6 (B6) and SJL/J genetic backgrounds. On the B6 background, $IgH^{[MOG]}$ mice showed an increased incidence of EAE, relative to WT, when immunized with whole MOG protein[16]. Notablyly, $IgH^{[MOG]}$ SJL/J mice developed EAE of greater severity than controls when immunized with the myelin-derived epitope proteolipid protein $(PLP)_{[139-154]}$[16], which induces a relapsing/remitting disease pattern in SJL/J background mice[58]. This suggested that the presence of MOG-reactive B cells could contribute to EAE pathology that was driven by a class II-restricted peptide. It was later shown that when $IgH^{[MOG]}$ mice were crossed to the 2D2 $MOG_{[35-55]}$

TcR-transgenic strain on the C57BL/6 background, the resulting double-transgenics spontaneously developed Devic's-like disease while single transgenic mice did not[17]. Similarly, IgH$^{[MOG]}$ x TCR^{1640} (ref [18]) and IgH$^{[MOG]}$ x 1C6 (ref [31]) double-transgenic mice, on the SJL/J and NOD backgrounds respectively, develop spontaneous EAE at a high rate of incidence[31]. These findings indicated that the collaboration of both myelin-specific B and T cells in the same animal could induce CNS autoimmunity; however, it was difficult to determine whether B or T cell-driven responses were initially responsible for disease induction in this model, and thus the nature of a putative collaboration between B cells and T cells in disease processes remained incompletely defined.

In our study, we actively immunized IgH$^{[MOG]}$ mice on NOD background with the class II-restricted peptide MOG$_{[35-55]}$. This permitted us to study the contribution of MOG-reactive B cells in a model of EAE that is initiated by CD4^{+} T cells. While WT NOD mice developed a gradual, chronic MOG$_{[35-55]}$-driven disease course, with advanced symptoms appearing as late as >100 days post immunization, we found that immunized IgH$^{[MOG]}$ NOD mice develop severe disease within a matter of weeks. Thus, by using a myelin-derived, class II-restricted, immunogen, we show that B cells augment EAE even when CD4^{+} T cells initiate disease. Interestingly, no differences in circulating anti-MOG IgG were identified between immunized between WT and IgH$^{[MOG]}$, suggesting that worsened disease in IgH$^{[MOG]}$ mice is not the result of increased production of encephalitogenic autoantibody.

The role of $CD4^+$ T cells in licensing peripheral B cell responses is well-established, and indeed the term “helper T cell” is derived from this function[59]. Th17 cells, in particular, can foster B cell responses by inducing class switching to inflammatory IgG1 and IgG2a[60] and by recruiting B cells to TLO structures[61]. Here, we provide evidence that the converse is also true, and that B cells may themselves shape Th17 responses. CNS-infiltrating $CD4^+$ T cells in $IgH^{[MOG]}$ mice showed significantly higher expression of IL-17 and GM-CSF, but not of IFNγ, indicating that Th17 responses are elevated in these mice. Further, CNS-infiltrating $IgH^{[MOG]}$ B cells showed increased expression of IL-23, an innate immune-associated cytokine that stabilizes the Th17 lineage and is required for the pathogenicity of Th17 cells[42,43], and *in vivo* blockade of IL-23 sharply reduced EAE in $IgH^{[MOG]}$ mice.

Overall, our findings show that B cells can play an important supportive role in facilitating pathogenic Th17 function and are consistent with a model by which bidirectional B:Th17 interactions are essential in CNS autoimmunity. Indeed, there is emerging evidence that B cells can promote Th17 responses. Both peritoneal $CD5^+B220^{lo}$ (ref [20]) and LPS-stimulated splenic $CD80^+CD86^+CD44^+$ (ref [21]) B cells can elicit Th17 differentiation. Further, production of IL-17 is defective from T cells taken from agammaglobulinemia patients that lack B cells[22] and therapeutic depletion of B cells with rituximab can reduce Th17 function in the context of MS[23] as well as in rheumatoid arthritis[24]. The mechanisms underpinning bidirectional B cell: T cell interactions remain to be fully elucidated.

Human B cells can secrete IL-23, and repression of this capacity is posited as a mechanism of action for interferon-beta in MS[44]. It was previously observed that peripheral B cells from naïve IgH$^{[MOG]}$ mice possess the capacity to secrete IL-23 (ref [62]); both upon pulsing with rMOG, and most strikingly upon co-culture with MOG$_{[35-55]}$-specific 2D2 T cells in the presence of either rMOG or MOG$_{[35-55]}$. B cell production of IL-23 in response to LPS is repressed by the inhibitory receptor Tim-1 (ref [63]). We now show that immunization with MOG$_{[35-55]}$ elicits IL-23 expression from CNS-infiltrating B cells *in vivo*, and that IL-23 is essential to both EAE and TLO formation from these animals.

Using mass cytometry, Brenner and colleagues found that PD1^{+}CXCR5^{-} CD4^{+} T cells accumulate in the inflamed synovium of RA patients. These Tph cells secrete B cell attractant factors such as CXCL13 and IL-21 and associate with B cells in the inflamed synovium, both in defined lymphoid aggregates as well as more diffusely. However, in contrast to Tfh cells, Tph are not defined by expression of the transcription factor Bcl6 [26]. While these cells are also observed in patients with lupus[51] and ANCA-associated vasculitis[64], their potential roles in murine models of autoimmunity remain obscure. We have found an enrichment of PD1^{+}CXCR5^{-} CD4^{+} T cells in the CNS, but not immune periphery, of immunized IgH$^{[MOG]}$ mice. These cells are Bcl6^{neg} and show increased expression of the Tph markers ICOS, CXCL13 and IL-21, relative to PD-1^{-} counterparts. Intriguingly, we find that the presence of PD-1^{+}CXCR5^{-} cells is highest in mice of peak EAE severity; Tph cells were previously shown to correlate with the severity of rheumatoid arthritis [26] and lupus [51]. Further, the accumulation of Tph cells in

the CNS is dependent on IL-23, revealing a heretofore unknown function of this cytokine.

In conclusion, we provide evidence that in the presence of a B cell repertoire that is skewed towards MOG, NOD-background mice develop unusually rapid and severe $CD4^+$ T cell-mediated EAE. Disease is dependent on IL-23, which is produced by B cells and is required for the augmented Th17 responses seen in these mice. Furthermore, these mice show accumulation of TLOs in their meninges that are again dependent on the presence of IL-23. Together, our findings support a critical role for myelin-reactive B cells in bolstering T cell-driven CNS autoimmunity in an IL-23-dependent manner.

Methods

Ethics

All mouse experiments and breedings were approved by the Animal Protection Committee of Université Laval (protocols 2021-820 and 2021-830, to M.R). Protocols and experiments involving human participants were approved by the Newfoundland Health Research Ethics Board (to C.S.M).

Animals

$IgH^{[MOG]}$ mice on the NOD background[31], and 1C6 mice[31-33], were obtained from Dr. Vijay Kuchroo (Brigham & Women's Hospital, Boston), and were maintained at the animal facility of the Centre de recherche du CHU de Québec-Université

Laval. NOD/ShiLtJ and NOD.*Scid* mice were purchased from Jackson Laboratories.

EAE induction and scoring

WT NOD and IgH$^{[MOG]}$ mice were immunized subcutaneously with 200µg MOG$_{[35-55]}$ (Feldan), emulsified in incomplete Freund's adjuvant (BD Difco) that was supplemented with 500 µg *M. tuberculosis* extract (BD Difco). On day 0 and day 2 post-immunization, mice received 200 ng pertussis toxin (List Biological Laboratories) intraperitoneally. Mice were monitored daily for signs of EAE, which were assessed using a semi-quantitative 0-5 scale: 0; no disease, 0.5; ruffled fur, 1; limp tail, 1.5; mild impairment in gait, 2; severe impairment in gait, 2.5; partial hind limb paralysis, 3; hind limb paralysis, 4; forelimb paralysis, 5; moribund [65]. Pre-onset analyses were conducted a minimum of 5 days post-immunization but before the onset of symptoms. For comparison of disease burden, area under curve was calculated for individual disease curves and was divided by the number of days in the protocol (AUC d^{-1}). For p19 blockade, mice were administered anti-p19 (clone G23-8) or istotype (rIgG1, clone HRPM; both BioXcell), 1 mg d^{-1} on d -1 and d6 [47].

Histopathology

Mice were euthanized and intracardially perfused with PBS. The spinal cord was extracted and fixed in 10% formalin and 30% sucrose prior to being embedded in paraffin. Five-to-seven-micron coronal sections of the spinal cords were collected

on superfrost microscope slides (using microtome, Leica Biosystems HistoCore Autocut) and dried overnight on a drying bench at 37°C. Slides were stored at room temperature in a slide storage box until staining was performed. Sections for Hematoxylin and Eosin (H&E) were deparaffinated with xylene, while toluene was used for Luxol Fast Blue (LFB) sections. Histology was performed as previously described [66], using standard H&E to visualize lymphocyte infiltration and LFB to stain myelin in order to visualize areas of demyelination. Briefly, stained slides were scanned at 20x using a brightfield microscope scanner (Aperio AT2 DX System), and representative RGB images of the cervical spine were acquired. Quantification of the staining was performed on Image J (software, v 1.53K) in a blinded manner. Images were split into separate single colour channels using the Colour Deconvolution plugin. Thresholding was performed on the single colour channels for hematoxylin and LFB, and an area fraction measurement was performed on the white matter of the spinal cord. Staining is expressed as the percent of total white matter that is stained.

Immunofluorescence

Immunofluorescence (IF) analysis was performed on flash-frozen brain tissue embedded in optimum cutting temperature medium (OCT). The tissue was cryo-sectioned (7-10um) and mounted onto positively charged slides. IF staining were performed with antibodies against surface immune antigens such as CD4, B220, CD45 and CD11c and in some cases against ECM antigens: Fibronectin,

PDGFRα/β simultaneously. Slides were imaged using a widefield inverted microscope (AxioObserver 7) and analysis was done using Image J software.

ELISA

Splenocytes and draining lymph nodes were isolated from NOD and IgH$^{[MOG]}$ mice 5d post-immunization. Cells were cultured at a concentration of 10×10^6 cells mL^{-1} in T cell media and stimulated, or not, with 10 mg mL^{-1} $MOG_{[35-55]}$. Supernatants were collected at d5 of the culture for the analysis of T cell cytokine production using a combination of commercially available antibodies (Biolegend). Briefly, the capture antibodies used were: purified anti-mouse IFNg (clone R4-6A2) and purified anti-mouse IL-17 (clone TC11-18H10.1). The detection antibodies used were: biotin anti-mouse IFNg; clone XMG1.2, biotin anti-mouse IL-17; clone TC11-8H4. Following the incubation with the avidin-horseradish peroxidase (Biolegend) and TMB substrate (Mendel Scientific), colorimetric readings were performed using a SpectraMax i3 Microplate Reader.

Measurement of serum immunoglobulin

Blood was collected from Igh[MOG] mice and WT mice at endpoint. Serum was collected by centrifuging blood samples at 2000g for 10min. Total anti-MOG IgG was quantified by using SensoLyte Anti-Mouse MOG(1-125) IgG Quantitative ELISA Kit (Anaspec).

Isolation of CNS-infiltrating mononuclear cells

Mice were euthanized and perfused intracardially with PBS. Brain and spinal cord were dissected from the skull and vertebral column respectively and were prepared as previously described [65]. Briefly, CNS tissues were digested with liberase (Roche) and DNAse I (Sigma) and cells were enriched using a 35% Percoll (GE Healthcare) gradient.

Flow cytometry

Single cell suspensions were obtained from spleens, lymph nodes and CNS of EAE mice. For detection of surface antigens, cells were stained with Fixable Viability Dye (eBioscience) and incubated with Fc Block (Biolegend) prior to staining with antibodies against surface antigens (CD45, CD4, CD8, CD19, CD11b, CD11c, B220, Ly6G, IgD, IgM, FAS, GL7, PD-1, CXCR5, ICOS, I-Ag^7, GFAP; details in following section). For detection of intracellular cytokines, cells were first stimulated with 50ng ml^{-1} PMA (Sigma), 1µM ionomycin (Sigma) and 1µL mL^{-1} GolgiStop (BD) for 4 hours at 37°C, prior to being labeled with viability indicator, Fc Block and relevant surface antigens as above. They were then fixed and permeabilized (Fixation Buffer and Intracellular Staining Perm Wash Buffer, both Biolegend) and stained for intracellular markers (IFN-γ, IL-17A, TNF-α, IL-6, GM-CSF, IL-12p40, IL-12p35, IL-23p19, IL-23; Bcl6, IL-21, CXCL13; details in following section). Samples were analyzed on a FACS Aria (BD) and data were analyzed using FlowJo software (Treestar).

Flow cytometry antibodies

The following monoclonal antibodies against mouse antigens were used: CD45, clone A20 (Biolegend); CD11b, clone M1/70 (eBioscience); CD11c, clone N418 (Biolegend); Ly6G, clone 1A8 (BD Biosciences); CD4, clone RM4-5 (eBioscience); CD8, clone 53-6.7 (Biolegend); CD19, clone 1D3 (eBioscience); B220, clone RA3-6B2 (eBioscience); IgD, clone 11-26c (eBioscience); IgM, clone 11/41 (eBioscience); FAS, clone 15A7 (eBioscience); GL7, clone GL-7 (eBioscience); PD-1, clone J43 (eBioscience), CXCR5, clone SPRCL5 (eBioscience); ICOS, clone C398.4A (eBioscience); GFAP, clone 1B4 (BD Biosciences); I-Ag^7, clone 39-10-8 (Biolegend); IFN-γ, clone XMG1.2 (eBioscience); TNF-α, clone MP6-XT22 (eBioscience); IL-17a, clone TC11-18H10.1 (Biolegend); GM-CSF, clone MP1-22E9 (eBioscience); IL-6, clone MP5-20F3 (eBioscience); IL-21, clone mhalx21 (eBioscience); IL-23 heterodimer, clone IC18871P (R&D Systems); IL-23p19, clone fc23pg (eBioscience); IL-12p35, clone 4D10p35 (eBioscience); IL-12p40, clone C17.8 (eBioscience); BCL6, clone IG191E/A8 (eBioscience); CXCL13, clone D58CX13 (eBioscience).

Immunofluorescence antibodies

The following monoclonal antibodies against mouse antigens were used: CD4 (RM4-5), B220 (RA3-6B2), CD11c (N418), CD45.2 (104), PDGFRα (APA5), and PDGFRβ (APB5), all of which are from eBioscience; and fibronectin (GW20021F, Sigma); smooth muscle actin (1A4, Sigma).

Antigen presentation assay

Single cell suspensions were obtained from the spleens of unimmunized WT and IgH[MOG] mice. Cells were labeled with CD43 (Ly-48) Microbeads (Miltenyi), and $CD43^+$ leukocytes (all leukocytes except resting B cells) were depleted on a magnetic MACS column (Miltyeni). Unlabelled $CD43^-$ cells were collected and were subsequently stained with anti-mouse CD19. $CD19^+$ B cells were purified using high-speed cell sorting. In parallel, $CD4^+$ T cells were purified from the spleens of 1C6 mice using mouse CD4 MicroBeads (Miltenyi) and labeled with CellTrace Violet (CTV; Thermo Fisher Scientific). CTV-labeled 1C6 $CD4^+$ T cells were cultured with B cells at a ratio of 1 CD4: 1 B, with 0, 1 or 10µg ml^{-1} $MOG_{[35-55]}$ for 72 hours. CTV dilution was assessed by flow cytometry.

Tfh culture

The protocol of Gao et al was adapted[67]. Briefly, $5x10^5$ splenocytes from NOD mice were stimulated 24h with LPS (1 µg mL^{-1}). $1x10^4$ $MOG_{[35-55]}$-specific 1C6 $CD4^+CD62L^{hi}$ T cells were then plated on top of the splenocytes with 1µg mL^{-1} $MOG_{[35-55]}$, plus 50 ng ml^{-1} IL-21 and 100 ng mL^{-1} of IL-6 (Tfh) or no additional cytokines (Th0) for 72h.

Analysis of CSF from MS-affected individuals

5mL of CSF was collected from consenting adult participants with MS at The Health Sciences Centre neurology clinic in St. John's, NL between July 2021 and

May 2022. For CSF immune phenotyping, 2.5mL of CSF was centrifuged for 10 minutes at 300g and the CSF was removed. The CSF cell pellet was resuspended in 100uL of flow buffer (1% bovine albumin serum, 2mM EDTA, 2mM sodium azide in PBS). The CSF cell suspension was added to a DURAclone IM Phenotyping BASIC tube (Beckman Coulter), mixed and incubated at 4°C for 30 minutes. The cells were washed with 4mL flow buffer, centrifuged at 300g for 5 minutes, decanted and resuspended in 100µL 2% paraformaldehyde. Data was acquired from the whole sample using a Cytoflex flow cytometer (Beckman Coulter) and analysed using FlowJo software. The $CD19^+$ cell count was expressed as a percentage of the total number of $CD45^+$ cells.

For measurement of CSF cell *Il23a* expression, 2.5 mL of human CSF was centrifuged at 300g for 10 minutes and the CSF supernatant was carefully removed. The CSF cell pellet was resuspended in 500ul of Trizol and stored at -80°C. Total RNA was extracted using chloroform extraction followed by an RNeasy Micro kit (Qiagen). 200ng of RNA was used to synthesize cDNA with the M-MLV Reverse Transcriptase kit (Invitrogen). *Il23a* transcript expression was quantified using *Il23a* (FAM labelled) and GAPDH (VIC labelled) Taqman probe/primer assays (Invitrogen), Fast Advanced Master mix (Invitrogen) and a ViiA7 Real-time PCR system (Applied Biosystems).

Statistical analysis

Comparisons between two groups were made by *t*-test. Fisher's exact test was used to test for differences in the frequency of mice attaining ethical endpoints. For calculation of Tph frequency at different disease stages, Tukey's multiple comparisons test was used. Two-tailed analyses were used in all instances. All error bars represent s.e.m. All statistical analyses were conducted using Prism software (GraphPad).

Abbreviations

Ab, antibody; CNS, central nervous system; CSF, cerebrospinal fluid; CTV, CellTrace Violet; DC, Dendritic cell; EAE, experimental autoimmune encephalomyelitis; EP, endpoint; GC, Germinal center; GM-CSF, granulocyte and macrophage colony stimulating factor; H&E, hematoxylin & eosin; IFN, interferon; Ig, immunoglobulin; IL, interleukin; LFB, Luxol fast blue; MHC, major histocompatibility complex; MOG, myelin oligodendrocyte glycoprotein; MS, multiple sclerosis; NOD, nonobese diabetic; PLP, proteolipid protein; preonset, PO; RR, relapsing/remitting; SP, secondary progressive; Tfh, T follicular helper; TLO, Tertiary lymphoid organ; TNF, tumor necrosis factor; Tph, T peripheral helper; WT, wildtype.

Declarations

Competing interests

M.R. held a research contract with Remedy Pharmaceuticals (2019-2020), with funds paid to the CHU de Québec. This contract is unrelated to the work in this manuscript.

Funding

The work was supported by a Biomedical Discovery Research Grant from the MS Society of Canada (#3781) and a CIHR Project Grant, to MR. RF and PG are supported by Ph.D. studentships from the Fonds recherche du Québec – Santé (FRQS). PMIAD was supported by a doctoral studentship from the Multiple Sclerosis Society of Canada. NB is Junior-2 scholar, and MR is a Senior scholar, of the FRQS.

Authors' contributions

RF directed the project conducted experiments and helped write the manuscript. PMIAD, NF, IA, APY and JB conducted experiments. RP, AR, BM, SL and OR conducted histological analyses. PG and NB assisted with serum detection of immunoglobulins. CSM contributed to writing of the manuscript. MR supervised the project and wrote the manuscript. All authors read and approved the final manuscript.

Acknowledgements

We thank Vijay Kuchroo for providing us with NOD-background IgH$^{[MOG]}$ and 1C6 mice respectively. We thank Françoise Morin for critical discussions; Vincent Desrosiers, Alexandre Brunet, Stéphanie Fiola for technical assistance with flow cytometry; and Kim Larose, Andrée Brisson, Mathieu Vallière-St-Amant, Cindy Ouellet and the veterinary service of Université Laval for technical assistance and collaboration regarding animal care.

Data availability statement

All datasets will be made upon reasonable request to the corresponding author.

Figure legends

Figure 1. Active immunization with MOG$_{[35-55]}$ induces severe EAE in IgH$^{[MOG]}$ mice. A. *Left,* Disease curves and linear regression of males (WT, n=10, IgH$^{[MOG]}$, n=10) and females (WT, n=10, IgH$^{[MOG]}$, n=10) immunized with MOG$_{[35-55]}$ and monitored for development of EAE. ****, p<0.0001. Representative of 2 experiments in each sex. *Right*, AUC analysis of disease curves for all mice studied (30 WT, 30 IgH$^{[MOG]}$). **B.** WT and IgH$^{[MOG]}$ spinal cords were sectioned and stained with hematoxylin & eosin (H&E; immune infiltration) and Luxol fast blue (LFB; myelin). Slides were canned at 10X magnification for quantification. WT, n=3, IgH$^{[MOG]}$, n=3. *, p<0.05, *t*-test. **C.** WT (n=3) and IgH$^{[MOG]}$ (n=3) mice

were immunized with $MOG_{[35-55]}$. LN cells were isolated at disease onset and IFNγ and IL-17 expression were determined by flow cytometry. Gated on live $CD4^+CD44^+$ events. **D.** Sera were collected from $MOG_{[35-55]}$-immunized WT (n=5) and $IgH^{[MOG]}$ (n=5) mice, and concentration of MOG-specific IgG was assessed by ELISA. n.s., not significant; *t*-test. *, p<0.05; ****, p<0.0001; n.s., not significant; linear regression analysis (**A**), *t*-test (**A-D**).

Figure 2. Increased presence of class-switched and inflammatory cytokine-positive B cells in the $IgH^{[MOG]}$ CNS. A. Mononuclear cells were isolated from the CNS of immunized WT (n=6) and $IgH^{[MOG]}$ (n=12) mice. Frequency and absolute numbers of $CD19^+$ B cells, $CD4^+$ and $CD8^+$ T cells, $Ly6G^+$ neutrophils, $CD11b^+CD11c^-$ macrophages and $CD11c^+$ dendritic cells were enumerated by flow cytometry. **B.** The frequency of immature ($IgM^{mid}IgD^{mid}$), mature ($IgM^{hi}IgD^{hi}$) and class-switched (CS; IgM^-IgD^-) B cells were assessed from WT (n=5) and $IgH^{[MOG]}$ (n=5) CNS. Gated on live $B220^+$ events. **C.** Expression of the indicated cytokines was assessed from WT (n=5) and $IgH^{[MOG]}$ (n=5) CNS B cells. Gated on live $CD19^+$ events. *, p<0.05; **, p<0.01; ***, p<0.001; ****, p<0.0001; n.s., not significant; *t*-test.

Figure 3. $IgH^{[MOG]}$ B cells exacerbate CNS-specific Th17 responses and show accumulation of meningeal TLOs. A. WT (n=5) and $IgH^{[MOG]}$ (n=5) were immunized with $MOG_{[35-55]}$ and CNS-infiltrating $CD4^+$ T cells were isolated at endpoints. Expression of the indicated cytokines was assessed by intracellular

flow cytometry. Gated on live $CD4^+$ events. *, $p<0.05$; **, $p<0.01$; n.s., not significant; *t*-test. **B.** Brain and spinal cord meningeal sections from $MOG_{[35-55]}$-immunized WT (n=3) or $IgH^{[MOG]}$ (n=3) mice were assessed by immunofluorescence (IF) for expression of B220 (red), CD4 (blue), and CD11c (green), and lymphocyte aggregates from the cerebellar meningeal compartment were enumerated. **C.** Assessment of the ECM near meninges in the cerebellum was determined by IF. Expansion on the meningeal ECM is shown by fibronectin (green) and PDGFRα/β (blue) which overlap with B220 B cell clusters. Dotted lines outline the meningeal membrane and (*) denotes vascular endothelium.

Figure 4. CNS $IgH^{[MOG]}$ B cells upregulate IL-23. A. WT (n=10) and $IgH^{[MOG]}$ (n=10) mice were immunized with $MOG_{[35-55]}$ and B cells were isolated from CNS tissues at endpoints. Expression of IL-12p35, IL-12p40 and IL-23p19 were assessed by intracellular flow cytometry. **B.** NOD (n=6) and $IgH^{[MOG]}$ (n=6) mice were immunized with $MOG_{[35-55]}$ and B cells were isolated from CNS tissues at endpoints. Expression of IL-23 heterodimer was assessed by intracellular flow cytometry. **C.** $IgH^{[MOG]}$ mice were immunized with $MOG_{[35-55]}$ and were treated on d (-1) and d6 with 1 mg anti-p19 (n=5) or rIgG1 isotype (n=5). Disease curves representative of 3 experiments. AUC calculations include all mice studied; anti-p19 (n=14) or rIgG1 isotype (n=14). **D.** Inflammatory foci (H&E) and demyelination (LFB) were quantified from cervical spine of immunized $IgH^{[MOG]}$ mice treated with anti-p19 (n=3) or rIgG1 isotype (n=3). **E.** IL-17 and IFNγ were

assessed from CNS-infiltrating $CD4^+$ T cells of mice from (**C**). *, p<0.05; **, p<0.01; ***, p<0.001; n.s., not significant; *t*-test.

Figure 5. Tph cells infiltrate the $IgH^{[MOG]}$ CNS. A. WT (n=6) and $IgH^{[MOG]}$ (n=6) mice were immunized with $MOG_{[35-55]}$ and T cells were isolated from spleen and CNS at endpoints. Expression of PD-1 and CXCR5 was assessed by flow cytometry. **B.** WT or $IgH^{[MOG]}$ mice were immunized and sacrificed at onset (n=4 each), peak (n=3 each), recovery (n=3 each). CNS-infiltrating $CD4^+$ T cells were isolated from these groups, as well as from mice that did not develop disease (n=4 each) and the frequency of PD-1^+CXCR5^- cells was assessed. **C.** Expression of IL-21, CXCL13 and ICOS was assessed from CNS-infiltrating $CD4^+$ T cells taken from immunized WT (n=6) and $IgH^{[MOG]}$ (n=6) mice, and expression between PD-1^- and PD-1^+ $CD4^+$ subpopulations was compared. **D**. Expression of IL-21, was compared between WT and $IgH^{[MOG]}$ CNS-infiltrating $CD4^+$ T cells using the same samples as in (**C**). *, p<0.05; **, p<0.01; ***, p<0.001; ****, p<0.0001; n.s, not significant; unpaired *t*-test (**A**, **D**), Tukey's multiple comparisons test (**B**), paired *t*-test (**C**).

Figure 6. Tertiary lymphoid organs accumulate in the meninges of $IgH^{[MOG]}$ mice in an IL-23-dependent manner. $IgH^{[MOG]}$ mice were immunized with $MOG_{[35-55]}$ and were treated on d -1 and d6 with 1 mg anti-p19 or rIgG1 isotype. **A.** Cerebellar meningeal sections from $MOG_{[35-55]}$-immunized $IgH^{[MOG]}$ mice, treated with isotype (n=6) or anti-p19 (n=6), were assessed for lymphocyte

clusters. **B.** ECM deposition underneath meningeal lymphoid aggregates were assessed as in **Fig. 3C**. **C.** T cells were isolated from spleen and CNS at endpoints from anti-p19 (n=5) or isotype-treated (n=5) mice. Expression of PD-1 and CXCR5 was assessed by flow cytometry. **D.** *Il23a* was assessed from CSF immune cells of MS-affected individuals (10 RRMS, 1 PPMS; 9 females, 2 males) by qPCR and was correlated to the frequency of $CD19^+$ B cells within the $CD45^+$ CSF leukocyte population of each patient. *, $p<0.05$; **, $p<0.01$. *t*-test (**A, C**); linear regression (**D**).

Supplemental Figure 1. A. WT NOD mice (n=5) were immunized with $MOG_{[35-55]}$ and were monitored for signs of EAE for 120d. **B.** Splenic and LN cells were isolated from immunized WT (n=3) and $IgH^{[MOG]}$ (n=3) cells at disease onset, and were stimulated with 10 μg mL^{-1} $MOG_{[35-55]}$. Supernatants were collected at d5 and IFNγ and IL-17 were assessed by ELISA. **C.** WT (n=8) and $IgH^{[MOG]}$ (n=8) mice were immunized with $MOG_{[35-55]}$, and $CD4^+$ T cells were isolated from cervical LNs at endpoints and assessed for expression of the indicated cytokines. **D.** WT or $IgH^{[MOG]}$ B cells were co-cultured with CellTrace Violet-labeled 1C6 T cells and pulsed, or not, with the indicated concentrations of $MOG_{[35-55]}$. Gate frequencies indicate the percentage of cells undergoing at least one cell division. Representative of triplicate cultures.

Supplemental Figure 2. A. Splenic immature, mature and CS B cells were assessed from the same mice as in **Figure 2B**. **B.** MHC class II ($I\text{-}Ag^7$)

expression was assessed from CNS B cells at endpoint from $MOG_{[35-55]}$-immunized NOD (n=5) or $IgH^{[MOG]}$ (n=5) mice. **C.** Germinal center B cells (GL-7^+Fas^+) were assessed from the spleens and CNS of $MOG_{[35-55]}$-immunized NOD (n=5) or $IgH^{[MOG]}$ (n=5) mice. *, $p<0.05$; ***, $p<0.001$, n.s., not significant.

Supplemental Figure 3. Dendritic cells ($CD11c^+$), astrocytes ($GFAP^+$), resting microglia ($CD45^{dim}CD11b^{dim}$) and activated microglia ($CD45^{hi}CD11b^{hi}$) were assessed for expression of p19 and p40 from the CNS of $MOG_{[35-55]}$-immunized WT (n=5) or $IgH^{[MOG]}$ (n=5) mice. DCs, microglia; n=5 each group; astrocytes, n=10 each group.

Supplemental Figure 4. A. Expression of Bcl6 was assessed from WT or $IgH^{[MOG]}$ PD-1^+CXCR5^- CNS-infiltrating T cells versus *in vitro* generated 1C6 Tfh or Th0. **B.** Expression of Bcl6 was assessed from CNS-infiltrating $CD4^+$ T cells taken from immunized NOD (n=6) and $IgH^{[MOG]}$ (n=6) mice, and expression between PD-1^- and PD-1^+ $CD4^+$ subpopulations was compared.

References

1. Kingwell, E. *et al.* Incidence and prevalence of multiple sclerosis in Europe: a systematic review. *BMC Neurol* **13,** 128 (2013).
2. Larochelle, C., Uphaus, T., Prat, A. & Zipp, F. Secondary Progression in Multiple Sclerosis: Neuronal Exhaustion or Distinct Pathology? *Trends in Neurosciences* **39,** 325–339 (2016).
3. Thompson, A. Overview of primary progressive multiple sclerosis (PPMS): similarities and differences from other forms of MS, diagnostic criteria, pros and cons of progressive diagnosis. *Mult. Scler.* **10 Suppl 1,** S2–7 (2004).

4. Baranzini, S. E. *et al.* B cell repertoire diversity and clonal expansion in multiple sclerosis brain lesions. *J. Immunol.* **163,** 5133–5144 (1999).
5. Owens, G. P. *et al.* Restricted use of VH4 germline segments in an acute multiple sclerosis brain. *Ann. Neurol.* **43,** 236–243 (1998).
6. Owens, G. P. *et al.* Single-cell repertoire analysis demonstrates that clonal expansion is a prominent feature of the B cell response in multiple sclerosis cerebrospinal fluid. *J. Immunol.* **171,** 2725–2733 (2003).
7. Magliozzi, R. *et al.* Meningeal B-cell follicles in secondary progressive multiple sclerosis associate with early onset of disease and severe cortical pathology. *Brain* **130,** 1089–1104 (2007).
8. Uccelli, A., Aloisi, F. & Pistoia, V. Unveiling the enigma of the CNS as a B-cell fostering environment. *Trends Immunol.* **26,** 254–259 (2005).
9. Genain, C. P., Cannella, B., Hauser, S. L. & Raine, C. S. Identification of autoantibodies associated with myelin damage in multiple sclerosis. **5,** 170–175 (1999).
10. Hauser, S. L. *et al.* B-cell depletion with rituximab in relapsing-remitting multiple sclerosis. *N. Engl. J. Med.* **358,** 676–688 (2008).
11. Kappos, L. *et al.* Ocrelizumab in relapsing-remitting multiple sclerosis: a phase 2, randomised, placebo-controlled, multicentre trial. *Lancet* **378,** 1779–1787 (2011).
12. Hauser, S. L. *et al.* Ofatumumab versus Teriflunomide in Multiple Sclerosis. *N. Engl. J. Med.* **383,** 546–557 (2020).
13. Montalban, X. *et al.* Ocrelizumab versus Placebo in Primary Progressive Multiple Sclerosis. *N. Engl. J. Med.* (2016). doi:10.1056/NEJMoa1606468
14. Lehmann-Horn, K., Kronsbein, H. C. & Weber, M. S. Targeting B cells in the treatment of multiple sclerosis: recent advances and remaining challenges. **6,** 161–173 (2013).
15. Rangachari, M. & Kuchroo, V. K. Using EAE to better understand principles of immune function and autoimmune pathology. *J. Autoimmun.* **45,** 31–39 (2013).
16. Litzenburger, T. *et al.* B lymphocytes producing demyelinating autoantibodies: development and function in gene-targeted transgenic mice. *J. Exp. Med.* **188,** 169–180 (1998).
17. Krishnamoorthy, G., Lassmann, H., Wekerle, H. & Holz, A. Spontaneous opticospinal encephalomyelitis in a double-transgenic mouse model of autoimmune T cell/B cell cooperation. **116,** 2385–2392 (2006).
18. Pöllinger, B. *et al.* Spontaneous relapsing-remitting EAE in the SJL/J mouse: MOG-reactive transgenic T cells recruit endogenous MOG-specific B cells. *J. Exp. Med.* **206,** 1303–1316 (2009).
19. Dang, A. K., Jain, R. W., Craig, H. C. & Kerfoot, S. M. B cell recognition of myelin oligodendrocyte glycoprotein autoantigen depends on immunization with protein rather than short peptide, while B cell invasion of the CNS in autoimmunity does not. *J. Neuroimmunol.* **278,** 73–84 (2015).
20. Zhong, X. *et al.* Reciprocal generation of Th1/Th17 and T(reg) cells by B1 and B2 B cells. *Eur. J. Immunol.* **37,** 2400–2404 (2007).

21. Wang, Y. & Rothstein, T. L. Induction of Th17 cell differentiation by B-1 cells. *Front Immunol* **3,** 281 (2012).
22. Barbosa, R. R. *et al.* Primary B-cell deficiencies reveal a link between human IL-17-producing CD4 T-cell homeostasis and B-cell differentiation. *PLoS ONE* **6,** e22848 (2011).
23. Bar-Or, A. *et al.* Abnormal B-cell cytokine responses a trigger of T-cell-mediated disease in MS? *Ann. Neurol.* **67,** 452–461 (2010).
24. van de Veerdonk, F. L. *et al.* The anti-CD20 antibody rituximab reduces the Th17 cell response. *Arthritis Rheum* **63,** 1507–1516 (2011).
25. Encinas, J. A. *et al.* QTL influencing autoimmune diabetes and encephalomyelitis map to a 0.15-cM region containing Il2. *Nat. Genet.* **21,** 158–160 (1999).
26. Rao, D. A. *et al.* Pathologically expanded peripheral T helper cell subset drives B cells in rheumatoid arthritis. *Nature* **542,** 110–114 (2017).
27. Mayo, L. *et al.* IL-10-dependent Tr1 cells attenuate astrocyte activation and ameliorate chronic central nervous system inflammation. *Brain* **139,** 1939–1957 (2016).
28. Farez, M. F. *et al.* Toll-like receptor 2 and poly(ADP-ribose) polymerase 1 promote central nervous system neuroinflammation in progressive EAE. **10,** 958–964 (2009).
29. Baker, D. *et al.* Autoimmune encephalomyelitis in NOD mice is not initially a progressive multiple sclerosis model. *Ann Clin Transl Neurol* **6,** 1362–1372 (2019).
30. Legroux, L. & Arbour, N. Multiple Sclerosis and T Lymphocytes: An Entangled Story. *J Neuroimmune Pharmacol* **10,** 528–546 (2015).
31. Anderson, A. C. *et al.* A transgenic model of central nervous system autoimmunity mediated by CD4+ and CD8+ T and B cells. *J. Immunol.* **188,** 2084–2092 (2012).
32. Yeola, A. P. *et al.* Endogenous T Cell Receptor Rearrangement Represses Aggressive Central Nervous System Autoimmunity in a TcR-Transgenic Model on the Non-Obese Diabetic Background. *Front Immunol* **10,** 3115 (2019).
33. Doss, P. M. I. A. *et al.* Male sex chromosomal complement exacerbates the pathogenicity of Th17 cells in a chronic model of central nervous system autoimmunity. *Cell Rep* **34,** 108833 (2021).
34. Obermeier, B. *et al.* Matching of oligoclonal immunoglobulin transcriptomes and proteomes of cerebrospinal fluid in multiple sclerosis. **14,** 688–693 (2008).
35. Barr, T. A. *et al.* B cell depletion therapy ameliorates autoimmune disease through ablation of IL-6-producing B cells. *J. Exp. Med.* **209,** 1001–1010 (2012).
36. Duddy, M. *et al.* Distinct effector cytokine profiles of memory and naive human B cell subsets and implication in multiple sclerosis. *J. Immunol.* **178,** 6092–6099 (2007).
37. Li, R. *et al.* Proinflammatory GM-CSF-producing B cells in multiple sclerosis and B cell depletion therapy. *Sci Transl Med* **7,** 310ra166 (2015).

38. Domingues, H. S., Mues, M., Lassmann, H., Wekerle, H. & Krishnamoorthy, G. Functional and pathogenic differences of Th1 and Th17 cells in experimental autoimmune encephalomyelitis. *PLoS ONE* **5,** e15531 (2010).
39. Howell, O. W. *et al.* Meningeal inflammation is widespread and linked to cortical pathology in multiple sclerosis. *Brain* **134,** 2755–2771 (2011).
40. deLuca, L. E. S. *et al.* Substrain differences reveal novel disease-modifying gene candidates that alter the clinical course of a rodent model of multiple sclerosis. *J. Immunol.* **184,** 3174–3185 (2010).
41. Pikor, N. B. *et al.* Integration of Th17- and Lymphotoxin-Derived Signals Initiates Meningeal-Resident Stromal Cell Remodeling to Propagate Neuroinflammation. *Immunity* **43,** 1160–1173 (2015).
42. McGeachy, M. J. *et al.* The interleukin 23 receptor is essential for the terminal differentiation of interleukin 17-producing effector T helper cells in vivo. *Nat. Immunol.* **10,** 314–324 (2009).
43. Haines, C. J. *et al.* Autoimmune memory T helper 17 cell function and expansion are dependent on interleukin-23. *Cell Rep* **3,** 1378–1388 (2013).
44. Ramgolam, V. S. *et al.* B cells as a therapeutic target for IFN-β in relapsing-remitting multiple sclerosis. *J. Immunol.* **186,** 4518–4526 (2011).
45. Langrish, C. L. *et al.* IL-12 and IL-23: master regulators of innate and adaptive immunity. *Immunol. Rev.* **202,** 96–105 (2004).
46. Nitsch, L. *et al.* Astrocyte-specific expression of interleukin 23 leads to an aggravated phenotype and enhanced inflammatory response with B cell accumulation in the EAE model. *J Neuroinflammation* **18,** 101–16 (2021).
47. Chen, Y. *et al.* Anti-IL-23 therapy inhibits multiple inflammatory pathways and ameliorates autoimmune encephalomyelitis. *J. Clin. Invest.* **116,** 1317–1326 (2006).
48. Quinn, J. L., Kumar, G., Agasing, A., Ko, R. M. & Axtell, R. C. Role of TFH Cells in Promoting T Helper 17-Induced Neuroinflammation. *Front Immunol* **9,** 382 (2018).
49. Zhang, F. *et al.* Defining inflammatory cell states in rheumatoid arthritis joint synovial tissues by integrating single-cell transcriptomics and mass cytometry. *Nat. Immunol.* **20,** 928–942 (2019).
50. Johnston, R. J. *et al.* Bcl6 and Blimp-1 are reciprocal and antagonistic regulators of T follicular helper cell differentiation. *Science* **325,** 1006–1010 (2009).
51. Bocharnikov, A. V. *et al.* PD-1hiCXCR5- T peripheral helper cells promote B cell responses in lupus via MAF and IL-21. *JCI Insight* **4,** (2019).
52. Schröder, J. B. *et al.* Immune Cell Activation in the Cerebrospinal Fluid of Patients With Parkinson's Disease. *Front Neurol* **9,** 1081 (2018).
53. Field, J. *et al.* A polymorphism in the HLA-DPB1 gene is associated with susceptibility to multiple sclerosis. *PLoS ONE* **5,** e13454 (2010).
54. Noronha, A., Toscas, A. & Jensen, M. A. Interferon beta decreases T cell activation and interferon gamma production in multiple sclerosis. *J. Neuroimmunol.* **46,** 145–153 (1993).

55. Duda, P. W., Schmied, M. C., Cook, S. L., Krieger, J. I. & Hafler, D. A. Glatiramer acetate (Copaxone) induces degenerate, Th2-polarized immune responses in patients with multiple sclerosis. *J. Clin. Invest.* **105,** 967–976 (2000).
56. Stüve, O. *et al.* Altered CD4+/CD8+ T-cell ratios in cerebrospinal fluid of natalizumab-treated patients with multiple sclerosis. *Arch. Neurol.* **63,** 1383–1387 (2006).
57. Myhr, K.-M., Torkildsen, Ø., Lossius, A., Bø, L. & Holmøy, T. B cell depletion in the treatment of multiple sclerosis. *Expert Opin Biol Ther* **19,** 261–271 (2019).
58. Vanderlugt, C. L. & Miller, S. D. Epitope spreading in immune-mediated diseases: implications for immunotherapy. **2,** 85–95 (2002).
59. Crotty, S. A brief history of T cell help to B cells. *Nat. Rev. Immunol.* **15,** 185–189 (2015).
60. Mitsdoerffer, M. *et al.* Proinflammatory T helper type 17 cells are effective B-cell helpers. *Proc. Natl. Acad. Sci. U.S.A.* **107,** 14292–14297 (2010).
61. Hartlehnert, M. *et al.* Bcl6 controls meningeal Th17-B cell interaction in murine neuroinflammation. *Proc. Natl. Acad. Sci. U.S.A.* **118,** (2021).
62. Lee, Y. *et al.* IL-21R signaling is critical for induction of spontaneous experimental autoimmune encephalomyelitis. *J. Clin. Invest.* **125,** 4011–4020 (2015).
63. Xiao, S. *et al.* Checkpoint Receptor TIGIT Expressed on Tim-1+ B Cells Regulates Tissue Inflammation. *Cell Rep* **32,** 107892 (2020).
64. Liu, Z. *et al.* Increased circulating PD-1hiCXCR5- peripheral T helper cells are associated with disease activity of ANCA-associated vasculitis. *Clin. Exp. Immunol.* **207,** 287–296 (2022).
65. Boivin, N., Baillargeon, J., Doss, P. M. I. A., Roy, A.-P. & Rangachari, M. Interferon-β suppresses murine Th1 cell function in the absence of antigen-presenting cells. *PLoS ONE* **10,** e0124802 (2015).
66. Rojas, O. L. *et al.* Recirculating Intestinal IgA-Producing Cells Regulate Neuroinflammation via IL-10. *Cell* **176,** 610–624.e18 (2019).
67. Gao, X., Wang, H., Chen, Z., Zhou, P. & Yu, D. An optimized method to differentiate mouse follicular helper T cells in vitro. *Cell. Mol. Immunol.* **17,** 779–781 (2020).

Figure 1.

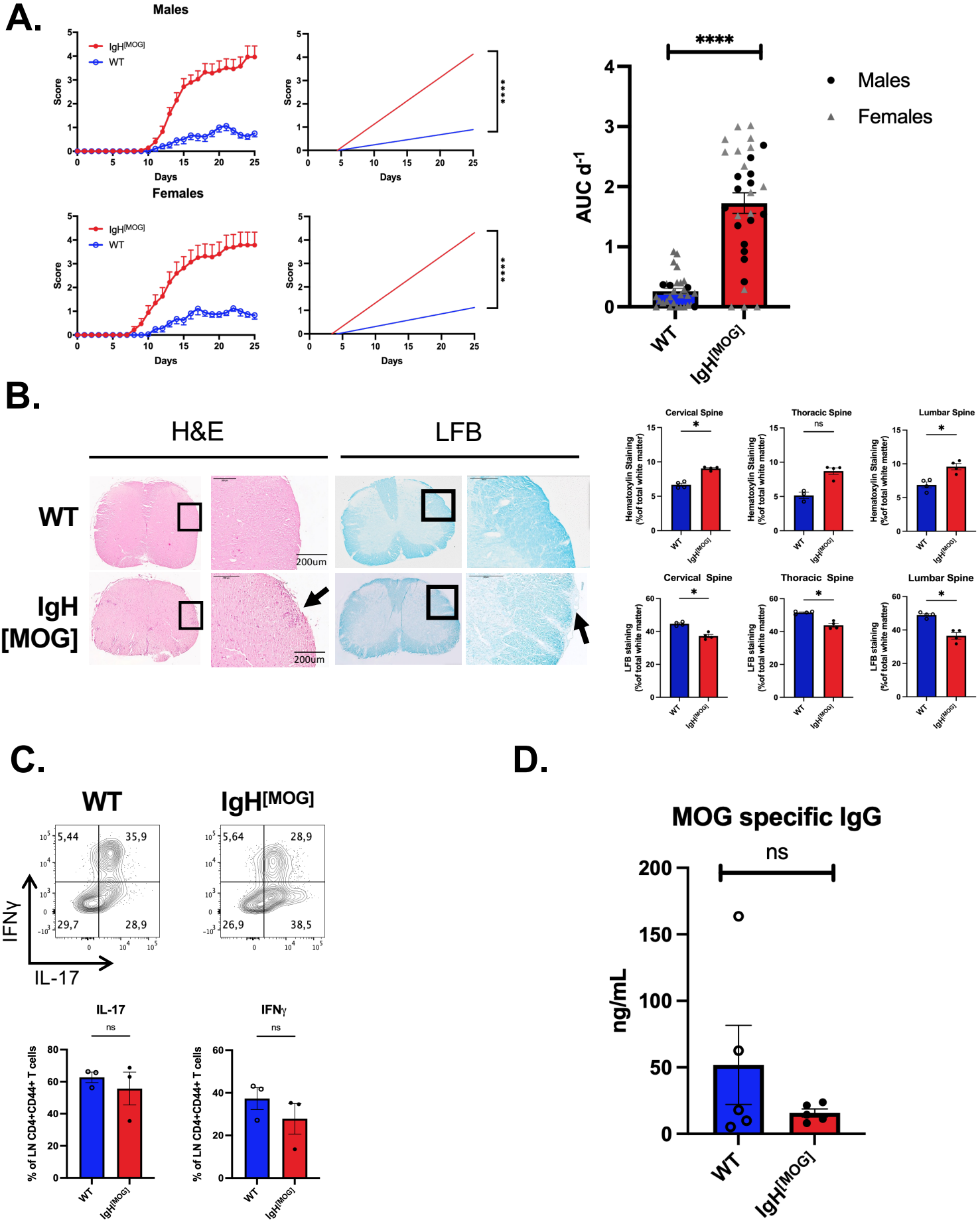
A.
Males
IgH[MOG]
WT
Score
Days
****
Females
AUC d-1
Males
Females
B.
H&E
LFB
WT
IgH [MOG]
200um
Cervical Spine
Thoracic Spine
Lumbar Spine
Hematoxylin Staining (%of total white matter)
LFB staining (%of total white matter)
ns
C.
WT
IgH[MOG]
5,44
35,9
29,7
28,9
5,64
28,9
26,9
38,5
IFNγ
IL-17
% of LN CD4+CD44+ T cells
D.
MOG specific IgG
ng/mL

Figure 2.

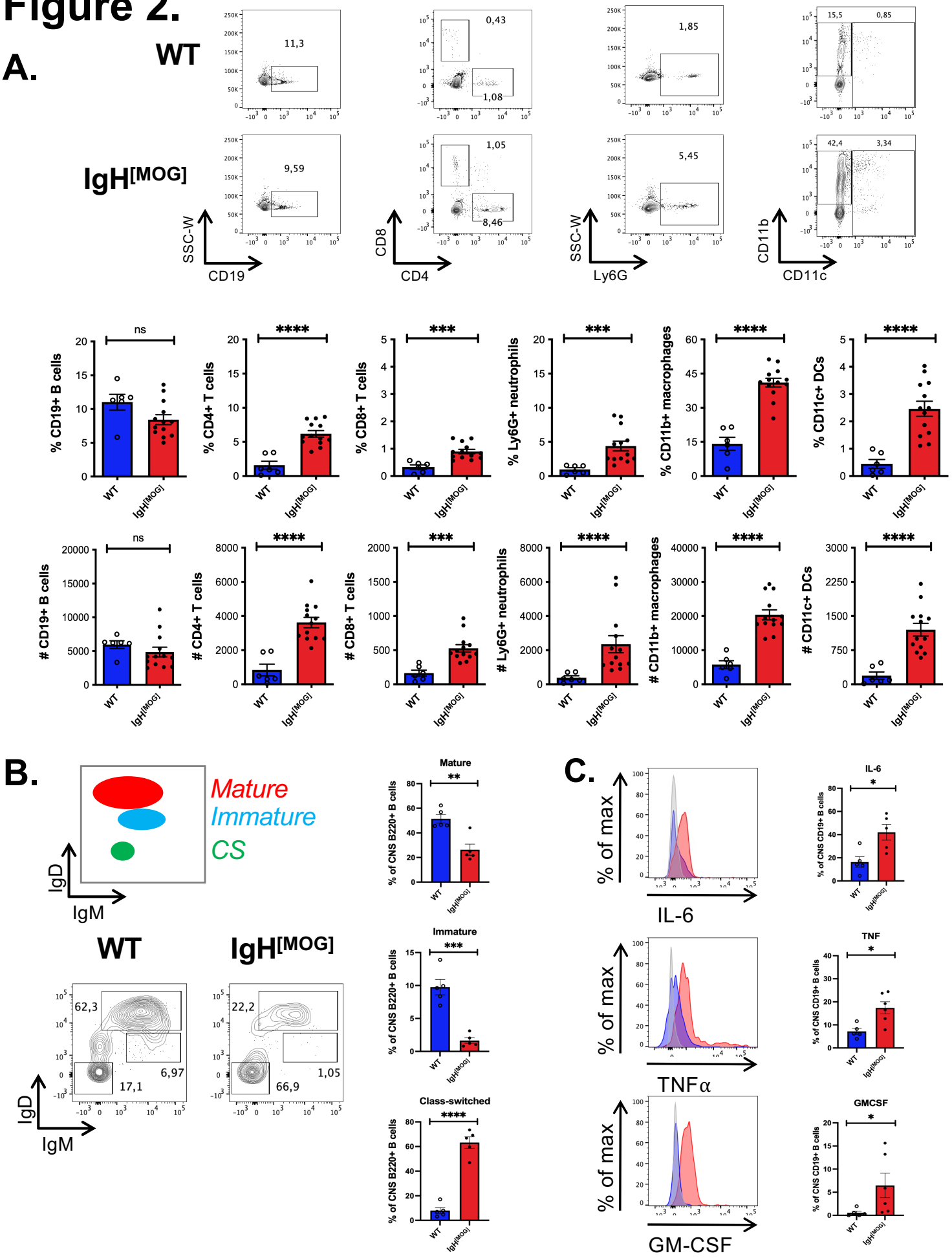
A.
WT
IgH[MOG]
11,3
9,59
0,43
1,08
1,05
8,46
1,85
5,45
15,5
0,85
42,4
3,34
SSC-W
CD19
CD8
CD4
SSC-W
Ly6G
CD11b
CD11c
% CD19+ B cells
% CD4+ T cells
% CD8+ T cells
% Ly6G+ neutrophils
% CD11b+ macrophages
% CD11c+ DCs
# CD19+ B cells
# CD4+ T cells
# CD8+ T cells
# Ly6G+ neutrophils
# CD11b+ macrophages
# CD11c+ DCs
ns
****
***
WT
IgH[MOG]
B.
Mature
Immature
CS
IgD
IgM
WT
IgH[MOG]
62,3
17,1
6,97
22,2
66,9
1,05
Mature
Immature
Class-switched
% of CNS B220+ B cells
**
***
****
C.
% of max
IL-6
TNFα
GM-CSF
% of CNS CD19+ B cells
*

Figure 3.

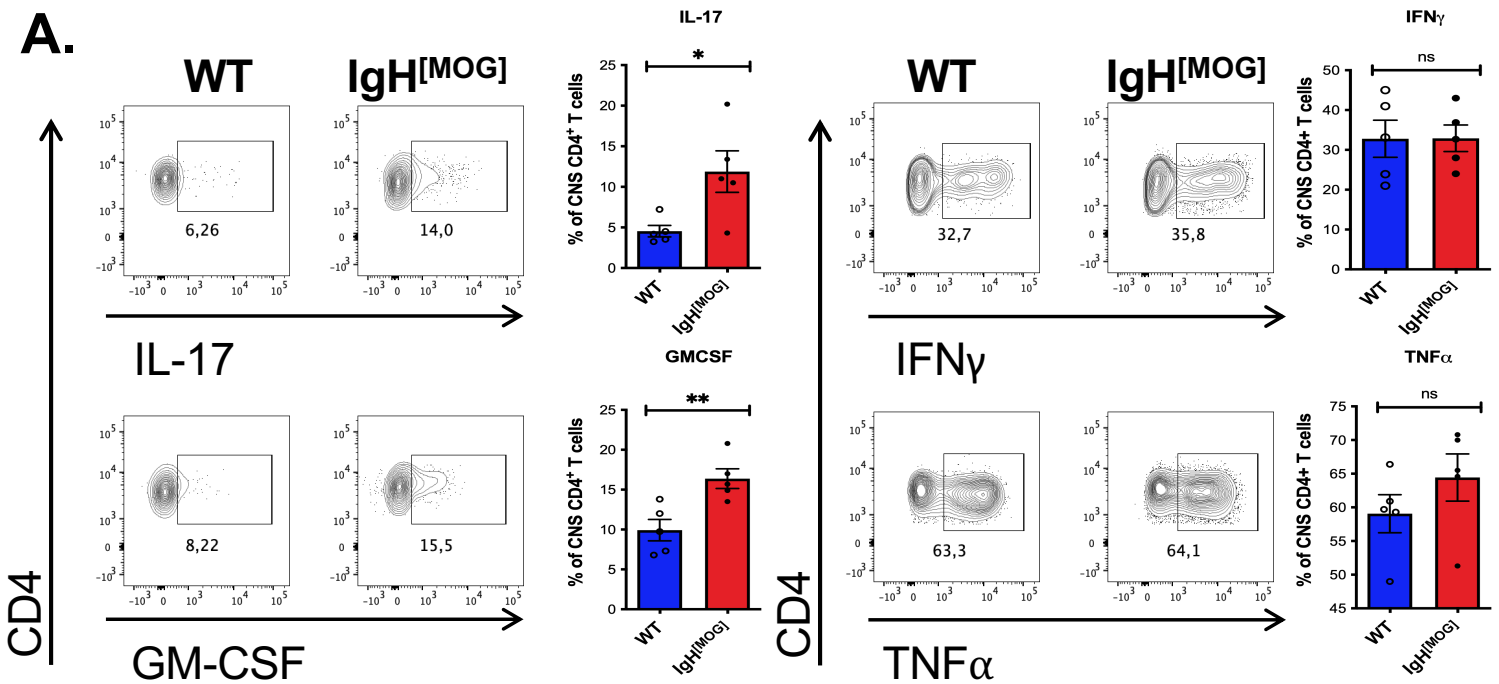
A.
WT
IgH[MOG]
6,26
14,0
IL-17
8,22
15,5
GM-CSF
CD4
IL-17
GMCSF
% of CNS CD4+ T cells
*
**
WT
IgH[MOG]
32,7
35,8
IFNγ
63,3
64,1
TNFα
CD4
IFNγ
TNFα
ns
ns

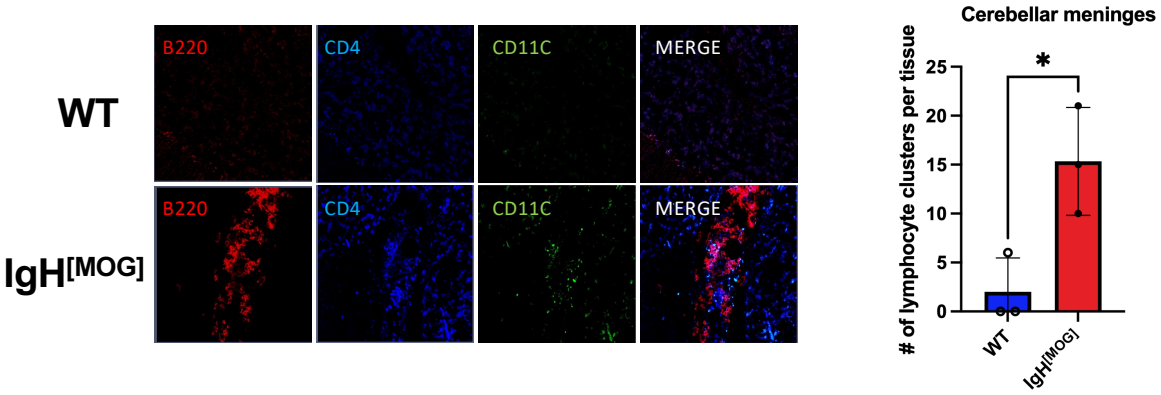
B.
WT
IgH[MOG]
B220
CD4
CD11C
MERGE
Cerebellar meninges
# of lymphocyte clusters per tissue
*
WT
IgH[MOG]

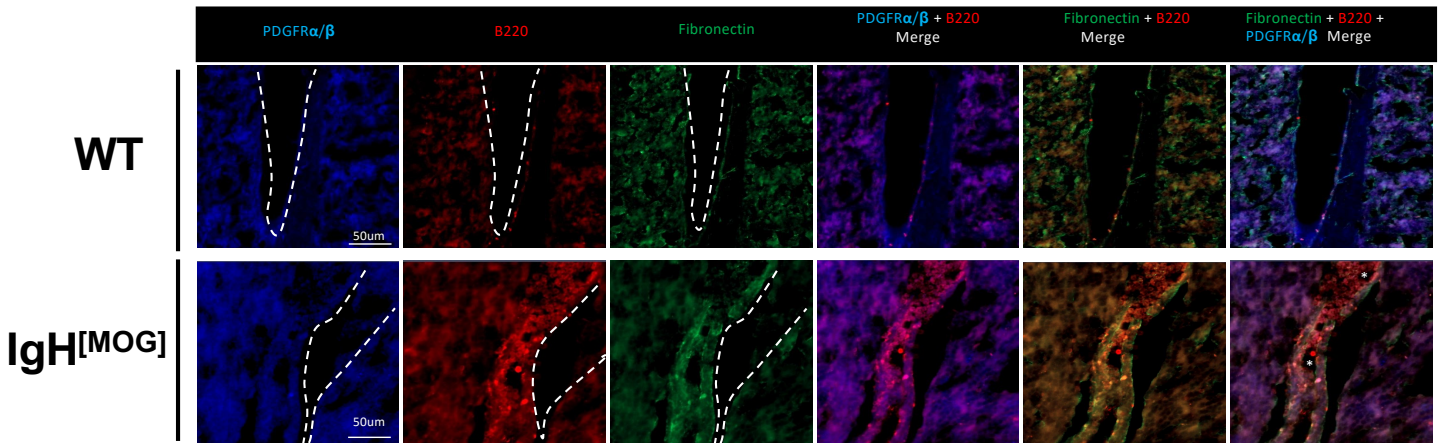
C.
PDGFRα/β
B220
Fibronectin
PDGFRα/β + B220 Merge
Fibronectin + B220 Merge
Fibronectin + B220 + PDGFRα/β Merge
WT
IgH[MOG]
50um
50um

Figure 4.

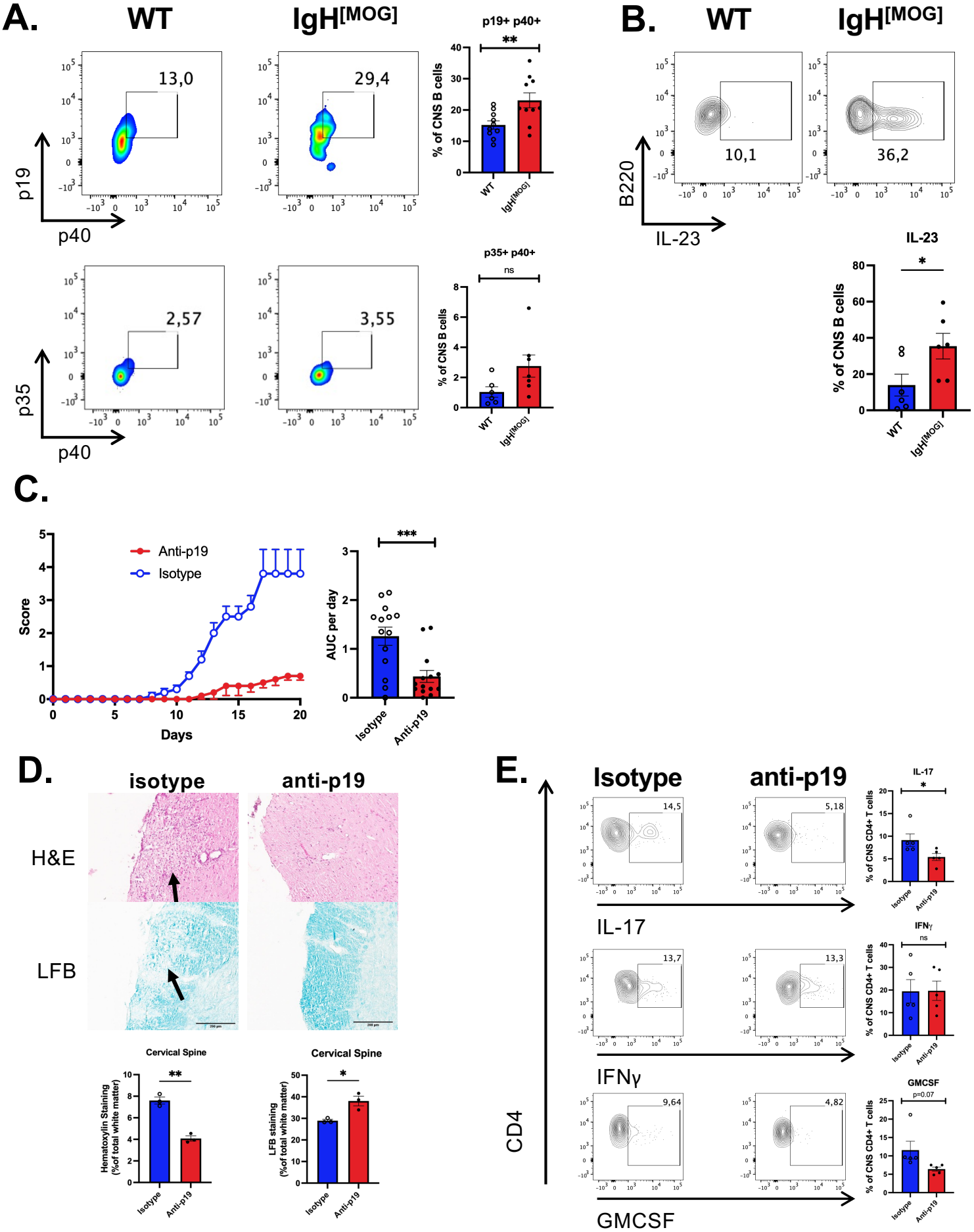
A.
WT
IgH[MOG]
13,0
29,4
p19
p40
p19+ p40+
**
% of CNS B cells
WT
IgH[MOG]
2,57
3,55
p35
p40
p35+ p40+
ns
B.
WT
IgH[MOG]
10,1
36,2
B220
IL-23
IL-23
*
C.
Anti-p19
Isotype
Score
Days
***
AUC per day
Isotype
Anti-p19
D.
isotype
anti-p19
H&E
LFB
Cervical Spine
Hematoxylin Staining (%of total white matter)
**
Cervical Spine
LFB staining (%of total white matter)
*
E.
Isotype
anti-p19
14,5
5,18
IL-17
IL-17
*
% of CNS CD4+ T cells
13,7
13,3
IFNγ
IFNγ
ns
9,64
4,82
GMCSF
GMCSF
p=0.07
CD4

Figure 5.

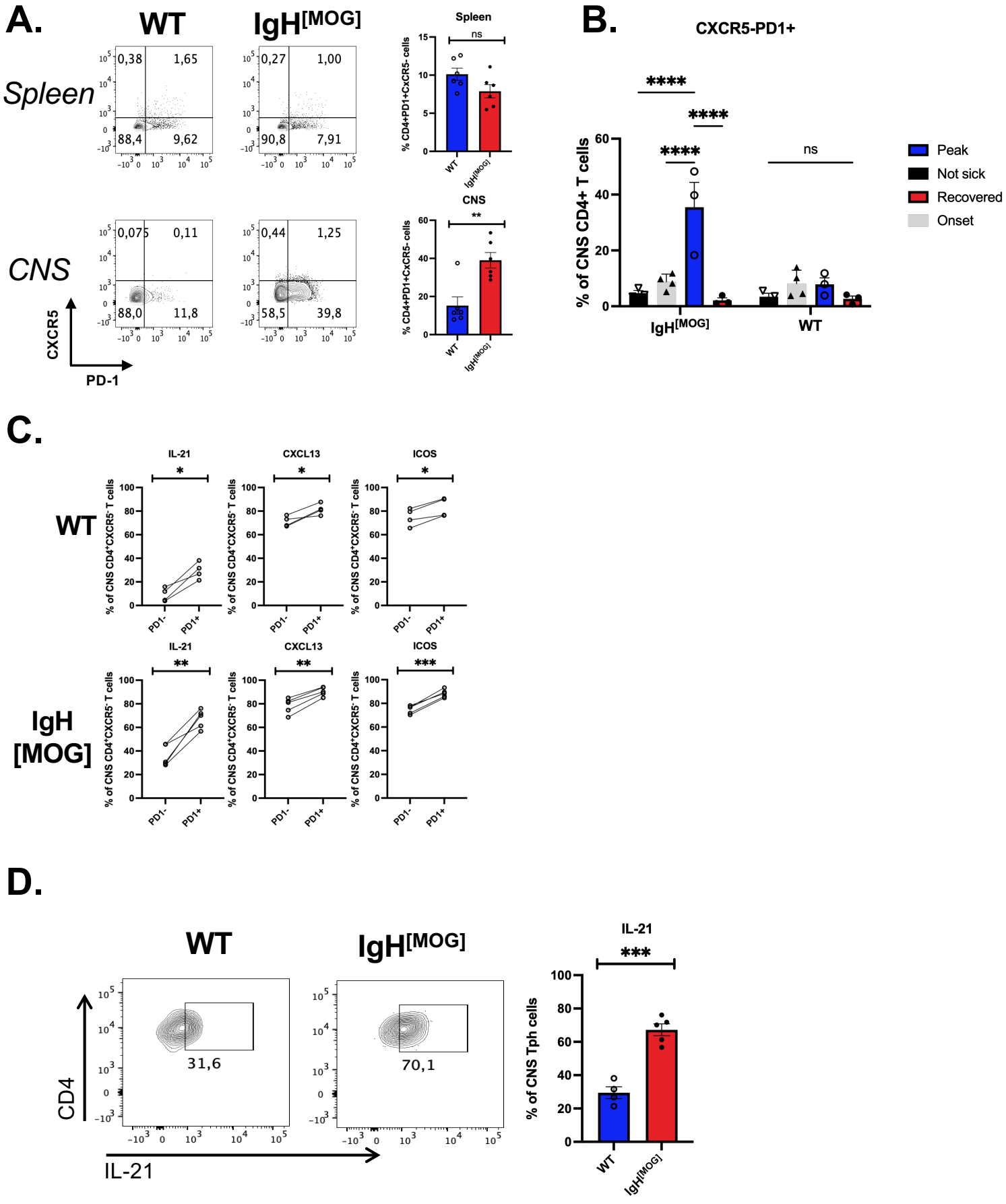
A.
WT
IgH[MOG]
Spleen
CNS
0,38
1,65
88,4
9,62
0,27
1,00
90,8
7,91
0,075
0,11
88,0
11,8
0,44
1,25
58,5
39,8
CXCR5
PD-1
Spleen
ns
% CD4+PD1+CxCR5- cells
CNS
**
% CD4+PD1+CxCR5- cells
WT
IgH[MOG]
B.
CXCR5-PD1+
****
****
****
ns
% of CNS CD4+ T cells
IgH[MOG]
WT
Peak
Not sick
Recovered
Onset
C.
WT
IgH [MOG]
IL-21
CXCL13
ICOS
% of CNS CD4+CXCR5- T cells
PD1-
PD1+
D.
WT
IgH[MOG]
31,6
70,1
CD4
IL-21
IL-21
***
% of CNS Tph cells
WT
IgH[MOG]

Figure 6.

A.

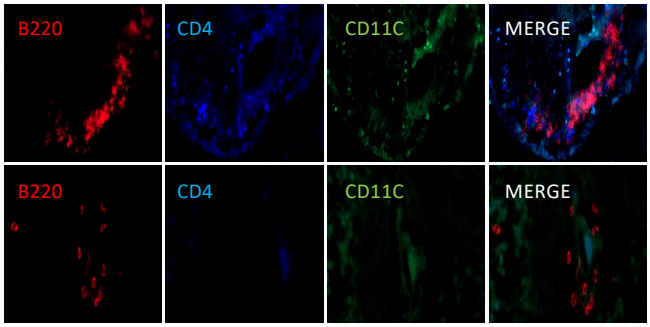

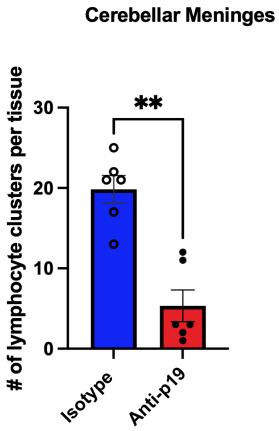

B.

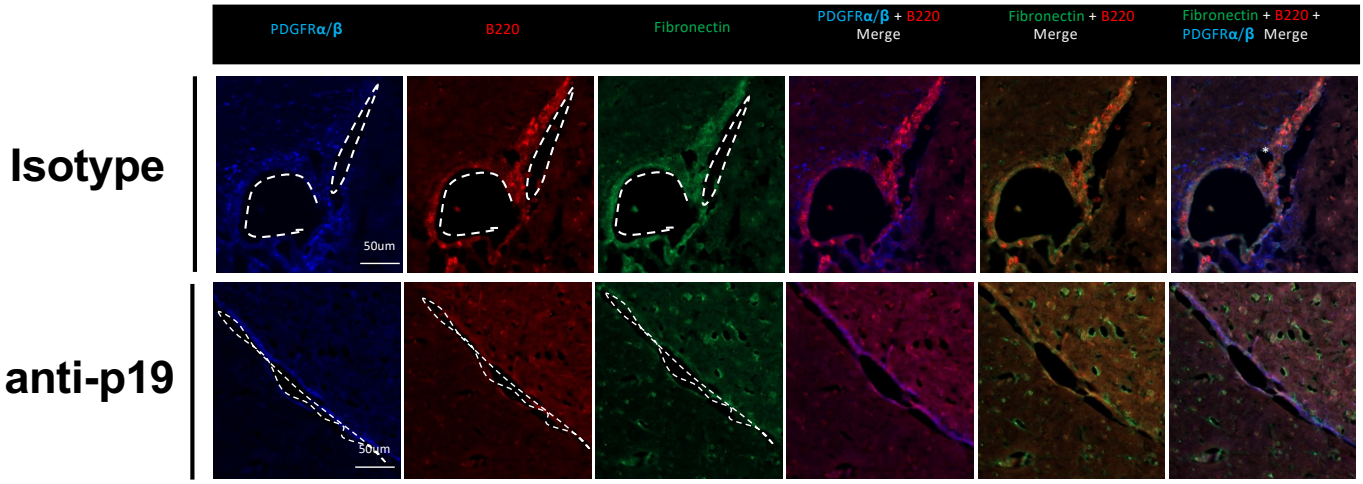

C.

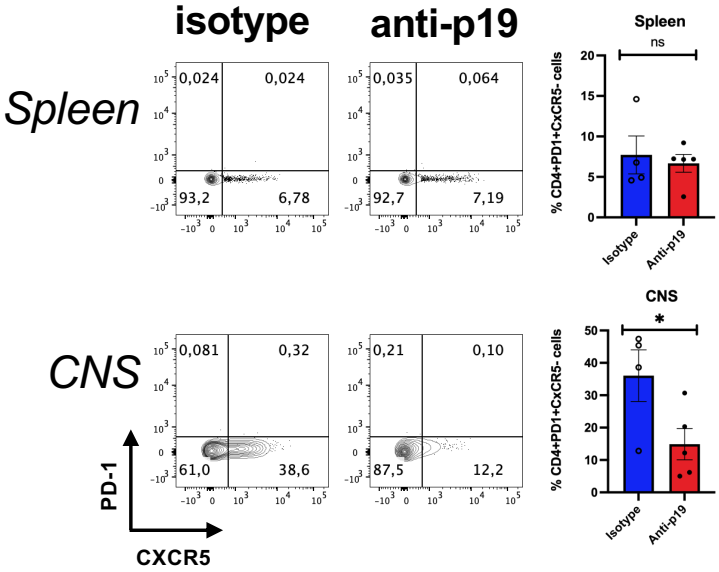
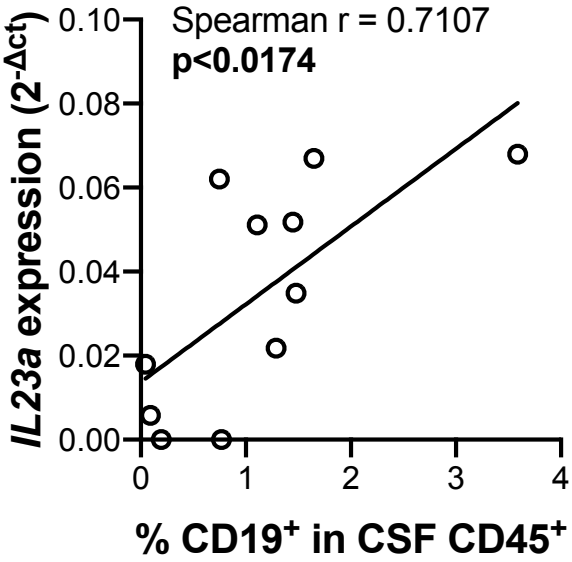
D.